JOURNAL OF SOLID STATE CHEMISTRY 62, 261–273 (1986)

Structural Changes Induced by Energetic Heavy-Ion Bombardment in $BaFe_{12}O_{19}$: HREM Investigation for Low Irradiation Doses*

M. HERVIEU, D. GROULT, AND B. RAVEAU

Laboratoire de Cristallographie, Chimie et Physique des Solides, U.A. 251, ISMRa-Université de Caen, 14032 Caen Cedex, France

AND G. FUCHS

CIRIL, Laboratoire commun CEA-CNRS, 14040 Caen Cedex, France

Received June 12, 1985; in revised form September 17, 1985

Monocrystalline and polycrystalline samples of hexaferrite $BaFe_{12}O_{19}$ irradiated with argon and krypton ion beams of 44 and 35 MeV per nucleon, respectively, have been investigated by HREM for doses close to 2×10^{13} and 2×10^{12} ions $\cdot$ cm^{-2}. Electron microscopy examinations of the samples placed in the low energy range ($0 \leq E < 0.6$ GeV for Ar and $0 \leq E < 0.9$ GeV for Kr) show several characteristic, morphologic, and crystallographic features involving numerous fractures, important bendings of the crystals, and extensive disorder leading to the loss of periodicity in the c direction. Typical induced defects have been observed and are believed to be associated with displacement cascades created by the primary ejected ions.

Introduction

The interaction of charged particles with solids is commonly used to modify the physical properties of the material. In this respect, ion implantations have been extensively studied. However, most of the studies concerning the irradiation effects in solids have been focused on metals, or semiconductors such as chalcogenides and a great number of these studies are limited to thin films. On the contrary, little is known about the behavior of oxides, especially in the bulk materials. The bombardment of such materials by energetic heavy ions has shown that the formation of nuclear tracks was possible if the energy deposited by electronic collisions is sufficiently high (*1*). The effects of atomic energy deposition have been studied less if one excepts the effects of ion implantation. The energy of the heavy-ion beams available at GANIL allows ion penetration depths up to 1 mm and makes easy a study of the radiation profile far from the surface, in bulk conditions. The first results recently obtained by irradiation of the hexaferrite $BaFe_{12}O_{19}$ by krypton and argon ions having an energy per nucleon of 35 and 44 MeV/A, respectively, are very promising (*2*). For the low-energy range ($0 \leq E < 0.9$ GeV for Kr and $0 \leq E < 0.6$ GeV for Ar), drastic variations of the magnetic properties have been observed; the electron microscopy study has shown a corresponding

* The irradiations were carried out at the National Laboratory GANIL, Caen, France.

0022-4596/86 $3.00

transition from a crystalline to an amorphous state involving damages of cascade displacement type. The present work deals with a high-resolution electron microscopy investigation of the structural changes induced in samples irradiated at relatively low doses, namely about 2×10^{12} and 2×10^{13} ions $\cdot$ cm^{-2} for Kr and Ar, respectively.

Experimental Procedures

The irradiation procedures have been previously described (*2*). Disks of about 3 and 8 mm diameter of $BaFe_{12}O_{19}$ were cut with a wire saw from single-crystal blocks oriented in the ⟨001⟩ direction and polycrystalline sintered samples. After being thinned by mechanical grindings to thicknesses ranging from 500 to 100 μm, they were stacked in sample holders fixed on the 77 K irradiation facility (IRABAT) of CIRIL (*3*) as pictured Fig. 1. The thickness of the disk stackings took into account the mean value of the projected ranges calculated from Hubert's and Northcliffe's tables (*4, 5*) namely 270 ± 0.5 μm and 650 ± 2 μm for Kr and Ar ions, respectively.

To study the effects of the ion irradiation along different directions, it was decided, in a first experiment, to divide the irradiated single crystal in small fragments; three

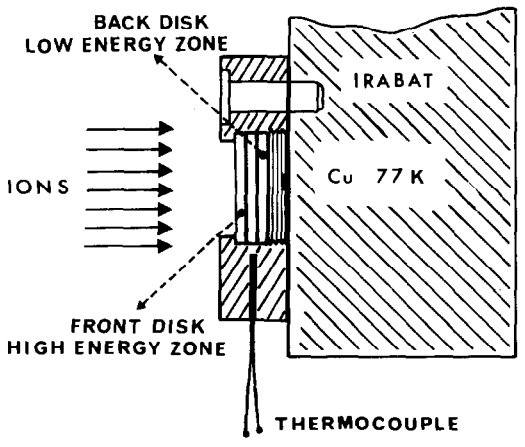

FIG. 1. Stacking of the disks in the sample holder.

planes were investigated: (001) planes which are perpendicular to the ion beam, and (110) and (100) planes which are parallel. This work concerns the samples which were located in the nuclear slowing down region where, in coming to rest, the incident particles interact predominantly with the target atoms. The electron microscopy samples were obtained from the irradiated disks by splitting in liquid nitrogen to avoid any mechanical effect. After being dispersed in *n*-butanol, numerous fragments were then collected on copper supported holey carbon films. The electron diffraction study was carried out with a microscope JEOL 100 CX, operated at 120 kV and fitted with an eucentric goniometer (±60°). The high-resolution electron microscopy study was performed with a double-tilt top entry goniometer (±10°) and with a high-resolution objective lens with a spherical aberration constant of 0.7 mm. The beam divergence was about 1×10^{-3} rad and the objective-aperture radius was 0.42 Å^{-1}. Thin flakes projecting over holes in the support film were selected and oriented for these observations.

HREM observation of nonirradiated samples. The presence of defects in hexagonal ferrites has been extensively studied (*6–11*). To interpret the defects observed in the irradiated ferrite $BaFe_{12}O_{19}$, a study of the nonirradiated sample was necessary as a reference.

For flat crystals symmetrically oriented with [001] parallel to the electron beam, images were characterized by 5.9-Å spaced white dots in a hexagonal array (Fig. 2). It must be pointed out that no defect was observed and that all the images recorded in the thin areas for this orientation are those of quasi perfect crystals. For the two other orientations, i.e., [100] and [110], the images appear as a fringe system in which the whitest ones have a spacing of 11.6 Å; this distance corresponds to $d_{00.2}$ of the *M* structure [*RSR*S**]. The observed defects corre-

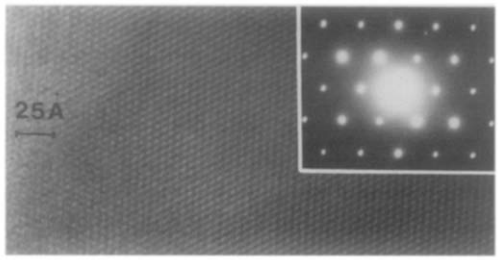

FIG. 2. High-resolution micrograph of (001) oriented microcrystal of nonirradiated material.

sponding to these orientations are the "classical" ones of the intergrowth structures and are quite in agreement with those previously mentioned in the barium ferrites (*6–12*): they principally consist in sequential faults, involving changes in the periodicity and in "superdislocations."

Results and Discussion

After irradiation the samples were characterized by numerous crystalline defects, strain contrasts, and considerable disorder. This effect of disorganization of the structure was also observed on the electron diffraction patterns whose diffraction spots covered a wide range extending from well defined spots to very disturbed dots.

(100) and (110) Planes

A typical field of view of the particles is shown in Figs. 3a and b. It can be seen that (001) reflexions, with $l = 2n + 1$, appear by multiple diffraction phenomena. Examination of the micrograph reveals several characteristic, morphologic, and crystallographic features of the irradiated samples and thoroughly illustrates our observations:

—Outbreak of fractures in the crystal forming slices which are 100–200 Å thick; they are always perpendicular to the *c* axis, i.e., to the ion beam. When the fracture is well initiated, as in upper left part of the micrograph, small misorientations are observed between the slices; in that example, the angle between their *c* axis is about 2°.

—Considerable bendings of the crystals: an angle of 20° is observed between the *c* axis of the upper and lower part of the micrograph. These "deviations" of the *c* axis from one part to another of the crystals are revealed on the electron diffraction patterns by a small arcing of the (*h0l*) spots.

—Extensive disorder leading to the loss of periodicity in the *c* direction; in some areas of the crystal the disorder appears to be complete and the contrast is that of amorphous material, whatever the focalization and the orientation of the sample under the electron beam may be. Such an example is observed in the middle of the micrograph, in the maximum bending zone of the crystal.

Such observations, i.e., bending of the crystal and numerous fractures, could be related to the lattice strain as shown in implanted garnet film (*13, 14*). We may assume, in view of the relative importance of the nonirradiated underlying back part of the disk, that the damaged part is in a state of lateral compression.

As another consequence of the deformation of the crystals, rapid local variations in contrast are observed, as pictured in Fig. 4a, depending upon defocus. Figure 4b shows an area of a crystal with a poor cristallinity. Moreover, two types of defects parallel to the *c* direction can be seen: loss of periodicity (lower right corner of the picture) and antiphase boundary (on the left side). Another type of defect, illustrated by the Fig. 5, must be noticed; it looks like a superdislocation, with a displacement of the lattice fringes across the defect, surrounded by a dark contrast due to the strain field. The peculiarity of this defect is its periodic occurrence in zones, perpendicularly to **c**, in regularly spaced zones.

(001) Planes

The electron diffraction patterns of the

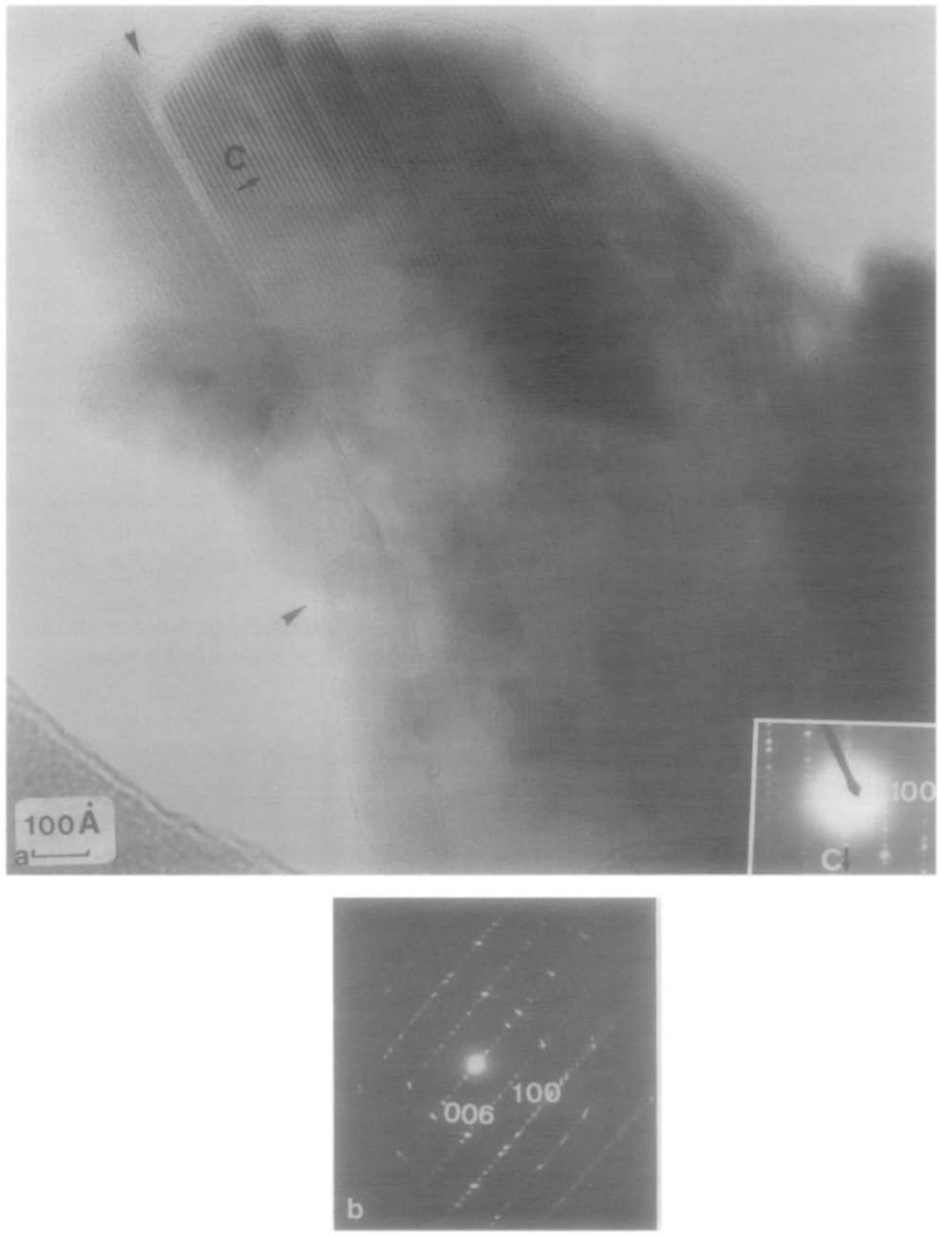

FIG. 3. Typical micrograph and electron diffraction pattern of the low-dose irradiated samples: fractures, bendings of the crystals, and extended defects are observed. (100) plane.

(001) plane show that most of the samples are more or less disordered but remain crystalline. Figure 6 presents, as an example, three electron diffraction patterns of (001) planes: the first one (a) is generally observed in a well crystallized zone whereas the third (c) corresponds to a disturbed zone, with misoriented lamellae. The HREM observations are consistent with these results: very few extended per-

fect crystals and very few amorphous particles were observed but most of the crystalline regions observed revealed many extended defects.

Micrographs 7 to 10 show the most significant features observed for Ar as well for Kr ions. The first of them (Fig. 7) presents at low magnification a crystal with, relatively, undamaged regions wherein the contrast corresponds to the expected hexagonal arrangement of white dots (A) surrounded by regions in which only two (B) or one (C) system of fringes are apparent. This area contains extended defects; the contrast of the defects changes with defocus and the lattice fringes exhibit bending or displace-

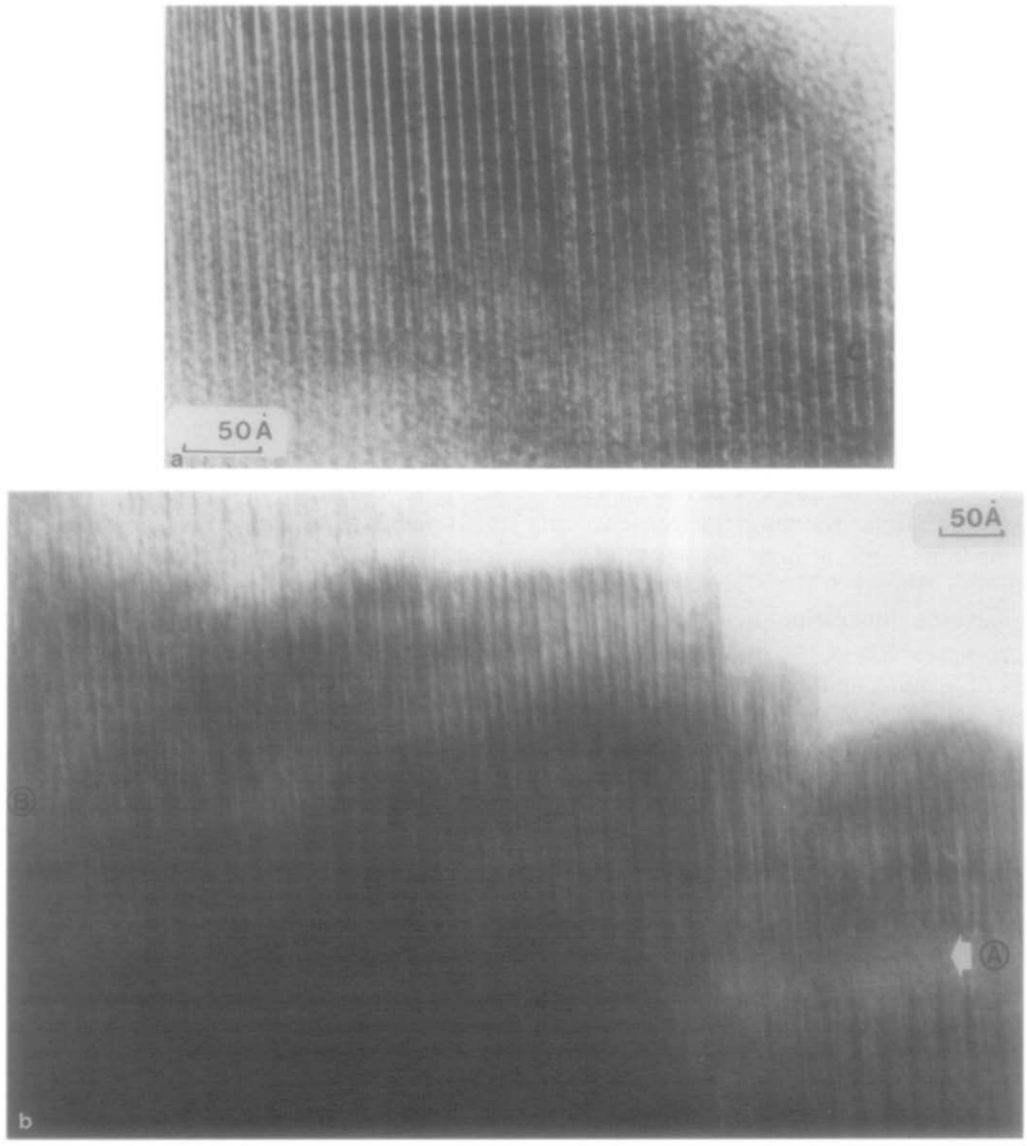

FIG. 4. Rapid local contrast variations (a) and local loss of periodicity are observed as consequences of the crystal deformations (b). [$1\bar{1}0$].

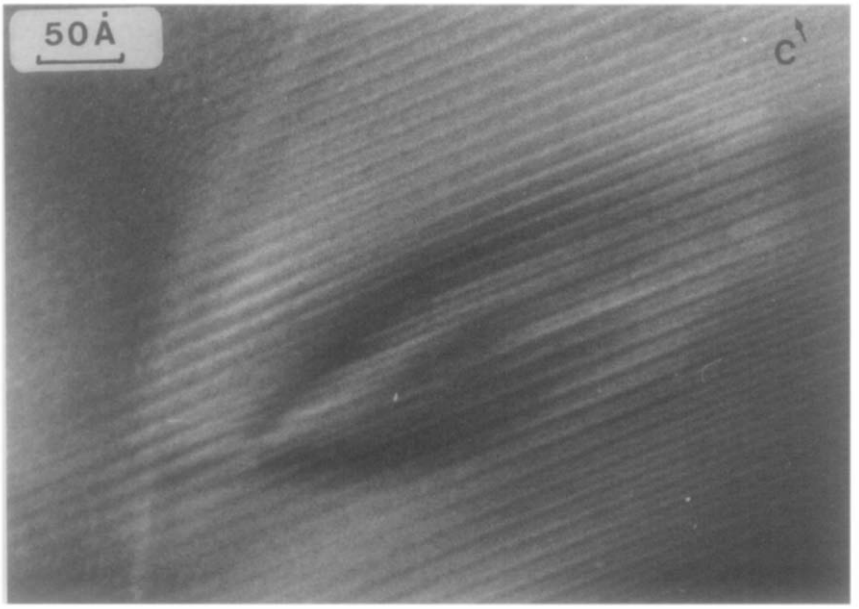

FIG. 5. Typical defect, parallel to (001), observed in the irradiated $BaFe_{12}O_{19}$.

ment across the defect; they sometimes disappear. Figure 8 is another example of such an appearance of numerous fragments in this orientation, showing the presence of dislocations and a high disorder of the structure. Figure 9 is an enlargement of a similar area illustrating these observations: in the upper left of the micrograph a small area of a quite undisturbed contrast is observed whereas in the middle, a network of dark contrast with shifting and bending of the fringes which disappear in some places can be seen.

The micrograph pictured Fig. 10 shows evidence of a more complex behavior. Beside the classical contrast expected for (001) plane (zone marked A) three principal zones labeled B, C, and D could be distinguished:

A strong modulation in the system of white fringes characterizes the zone B. One period contains three rows of dots; two are white and one is dark. This type of modulation is the most frequently observed, generally accompanied by APB parallel to ⟨110⟩. These superstructures appear in domains of

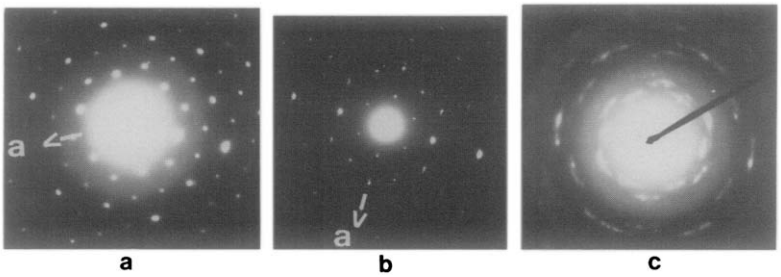

FIG. 6. Electron diffraction patterns of (001) planes: from well crystallized (a) to disturbed (c) with misorientation of the splitted fragments.

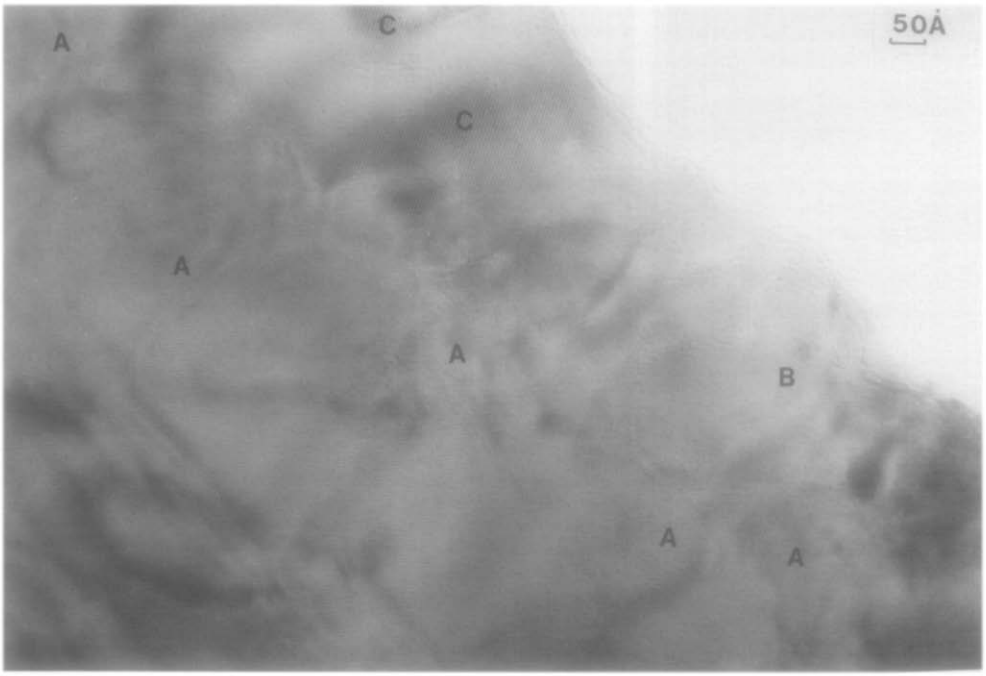

FIG. 7. Image of not very disturbed area exhibiting extended defects. (001) plane.

FIG. 8. High-resolution image of a region showing disorder of the structure; lattice fringe system is unidimensional in this part of the crystal. (001) plane.

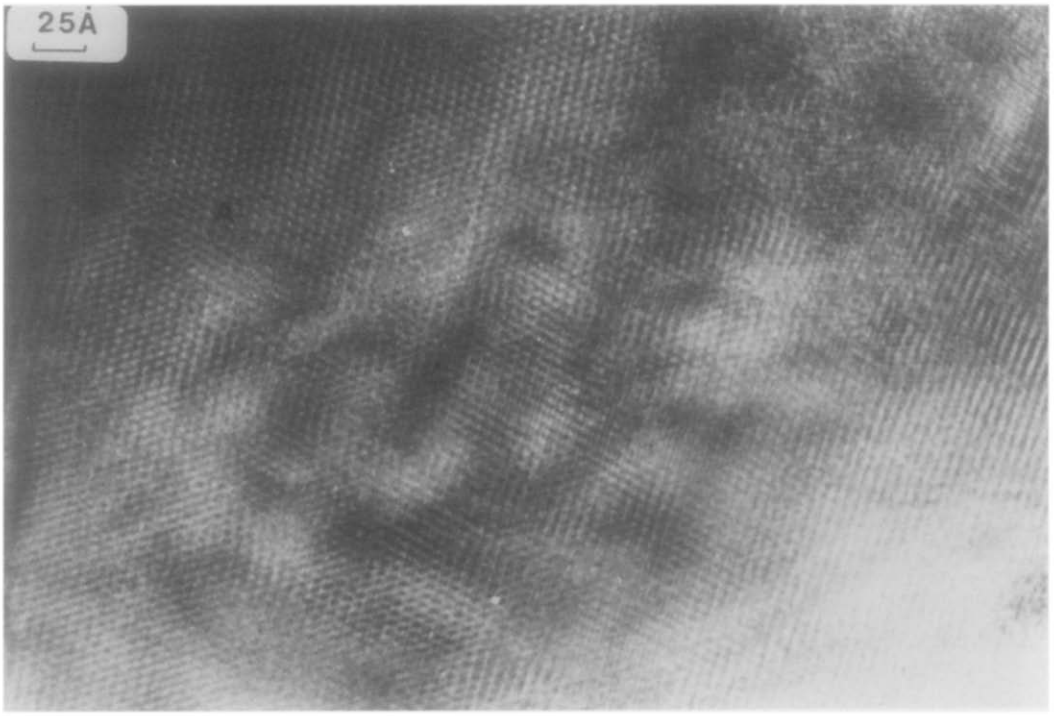

FIG. 9. Enlargement of an area showing bending and displacement of the lattice fringes. (001) plane.

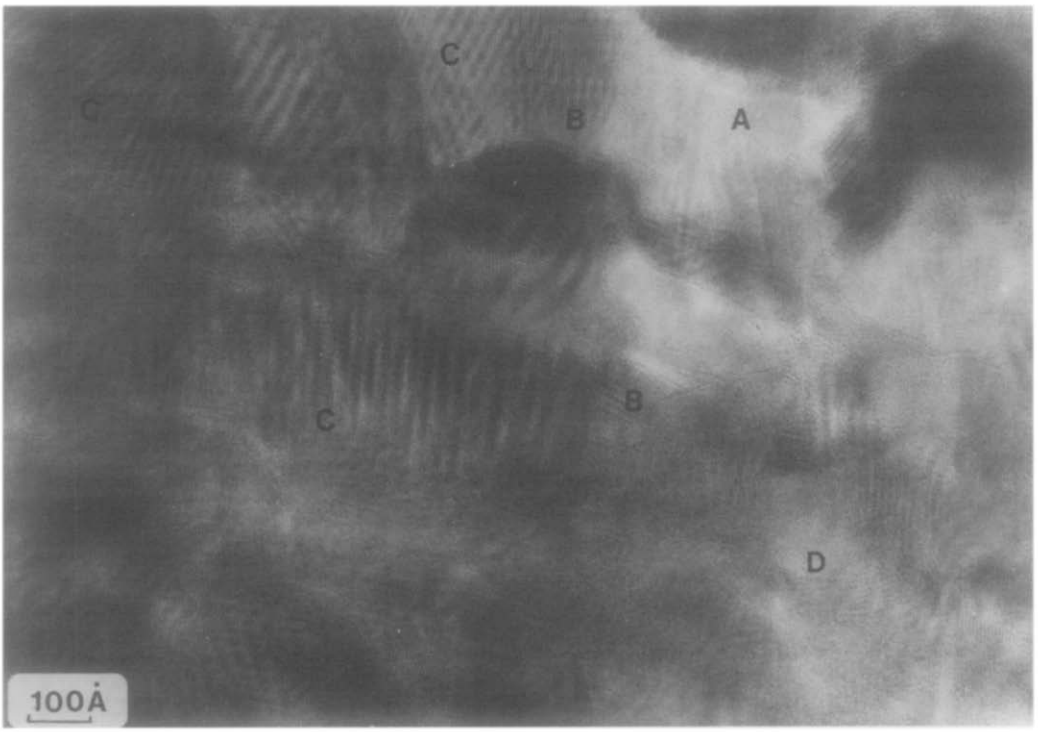

FIG. 10. High-resolution image of a complex area with intensity modulations, superstructures and moirés. (001) plane.

few hundred angstroms diameter. The other observed superstructures correspond to an orthorhombic cell ($b_0 \sim a_H\sqrt{3}$, $a_0 \sim a_H$).

Numerous moiré fringe systems resulting in differences in the layers perpendicular to the electron beam can be observed in zones C. They are related to the presence of de-

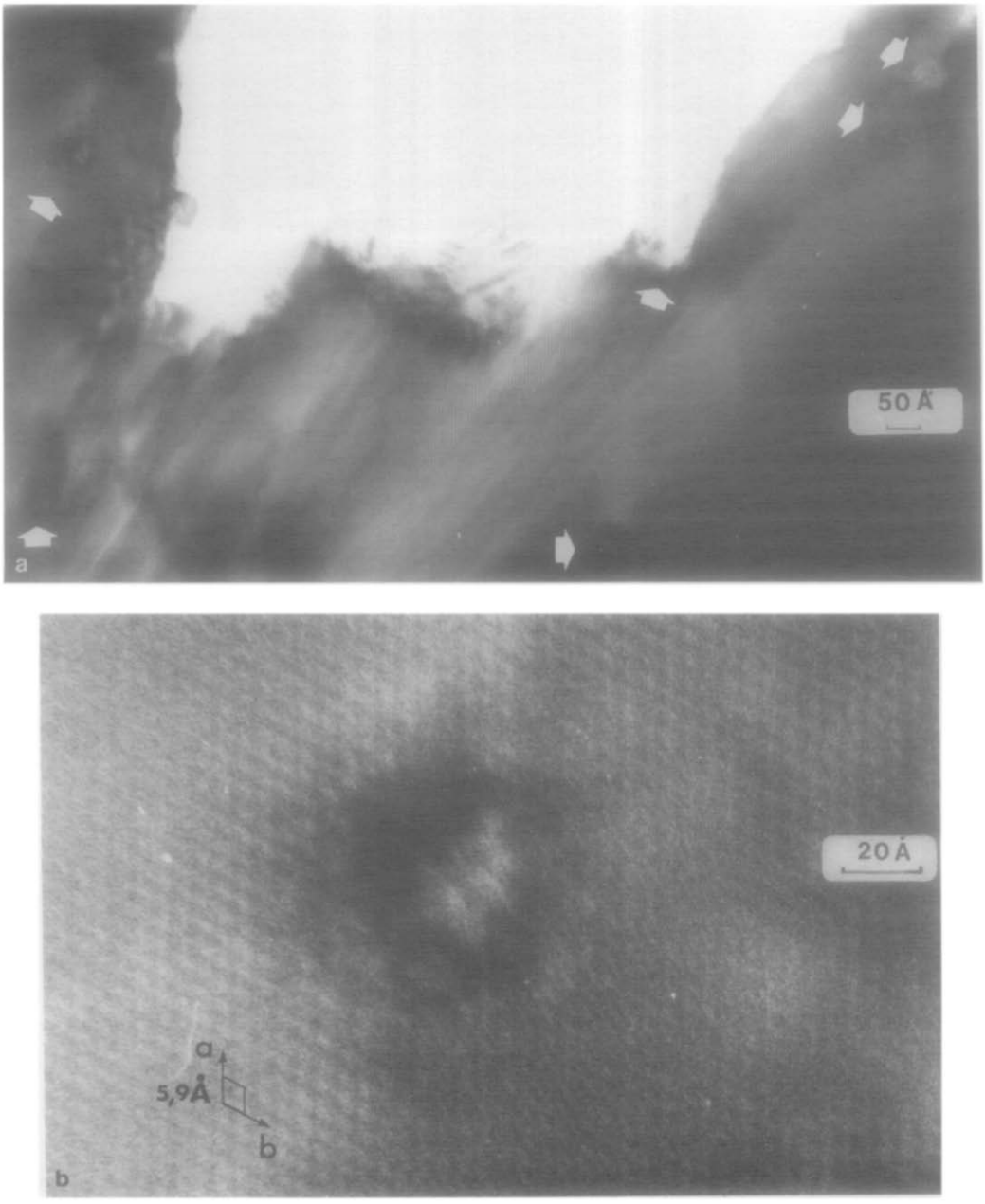

FIG. 11. High-resolution image (a) and enlargement (b) of a defect suggesting a displacement cascade created by the primary ejected ions. (001) plane.

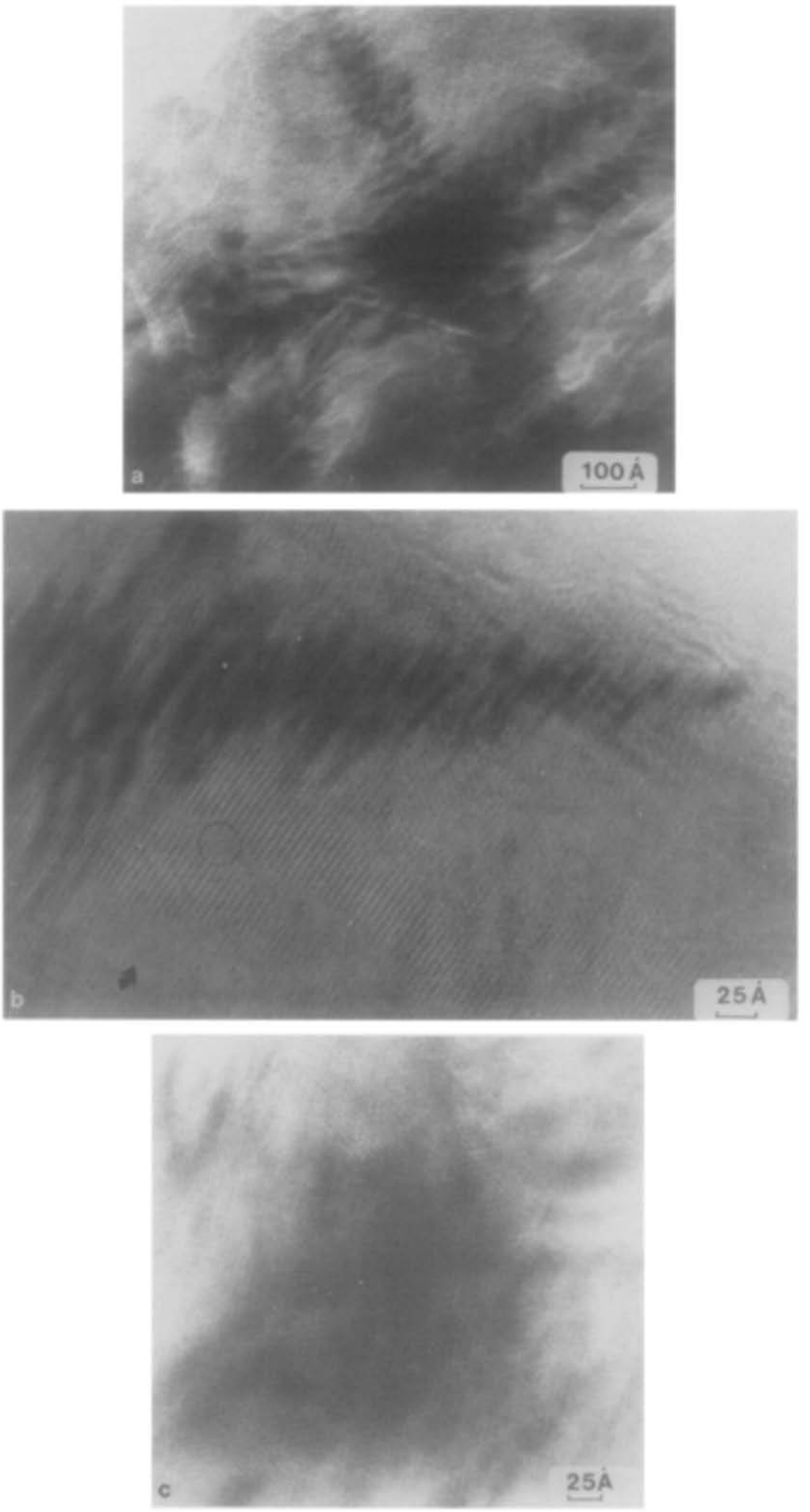

FIG. 12. (a) Low-magnification of a defect which appears as a "dark cross." Enlargements of one branch (b) and of the core (c). (001) plane.

fects such as stacking faults or misalignments like that observed in (100) planes. The distances between the moiré fringes vary from one zone to another; the following distances are more often encountered: ~12.2, ~19, and ~30.5 Å. Domains as the one outlined by an arrow (upper middle of the micrograph) correspond to a hexagonal arrangement of the moiré dots and could be explained by the overlap of different layers characterized by superstructures along the a axis.

In several parts of the crystals corresponding to zones marked (D), fringes with differents spacings forming domains can be seen but no proof of superstructure or precipitate can be put forward. Measurements on enlarged micrographs showed that distances and angles are coherent with the observation of (102) or (101) fringes.

Beside this characteristic aspect of the irradiated samples, one must notice some defects which depend on the nature of the ion beam, Ar or Kr. The first ones, pictured in Fig. 11a are observed in Kr-irradiated samples ($\phi t = 2 \times 10^{12}$ cm^{-2}) in quasi-undisturbed regions. They consist of voids which appear, at high magnification (Fig. 11b), to have a lighter core without fringes, corresponding to a disorganized area, surrounded by a darker outer shell. The occurrence of such disordered microregions of about 60 Å diameter, is believed to be associated with the displacement cascades created by the primary ejected ions. Taking into account the density of the defects (about 5×10^{10} cm^{-2}), the ion dose ($\phi t = 2 \times 10^{12}$ cm^{-2}) and the thickness of the sample (about 50 nm) one may deduce a mean event cross section of 5×10^4 barns in accordance with the value which can be calculated (2×10^4 barns) if one assumes a threshold energy of 1 keV for the primary knock-on atom inducing a cascade.

Two other types of defects have been observed in Ar-irradiated samples ($\phi t = 2 \times 10^{13}$ cm^{-2}). One of them is presented in Fig. 12. It looks like a dark "cross" whose

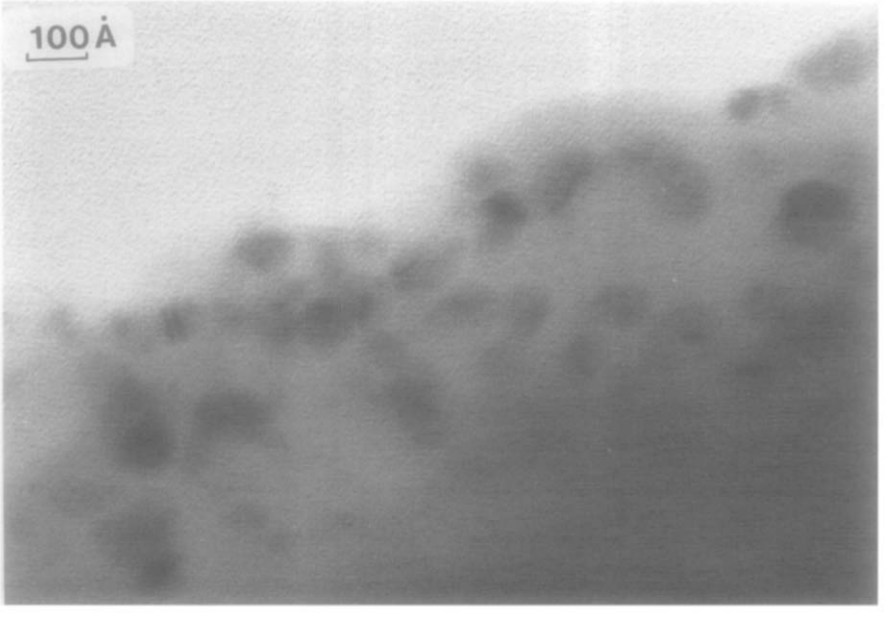

FIG. 13. Low-magnification image of irradiated $BaFe_{12}O_{19}$ showing blobs in amorphous material. (001) plane.

striped branch are generally parallel to ⟨100⟩ or ⟨110⟩ directions with lengths ranging from 400 to 600 Å. Micrographs 12b and 12c are enlargements of one branch and of the core of such a cross respectively. They show that the formation of the cross occurs in disturbed regions but without involving the amorphization of the bulk. As illustrated by the Fig. 12, the branch of the cross is located in a part of the crystal where the contrast consists in a one-dimensional system of fringes which exhibit dislocations and shiftings (black circle) and sometimes disappear (black arrow). In the striped dark contrast, the lattice fringes appear as nonstraight and poorly resolved.

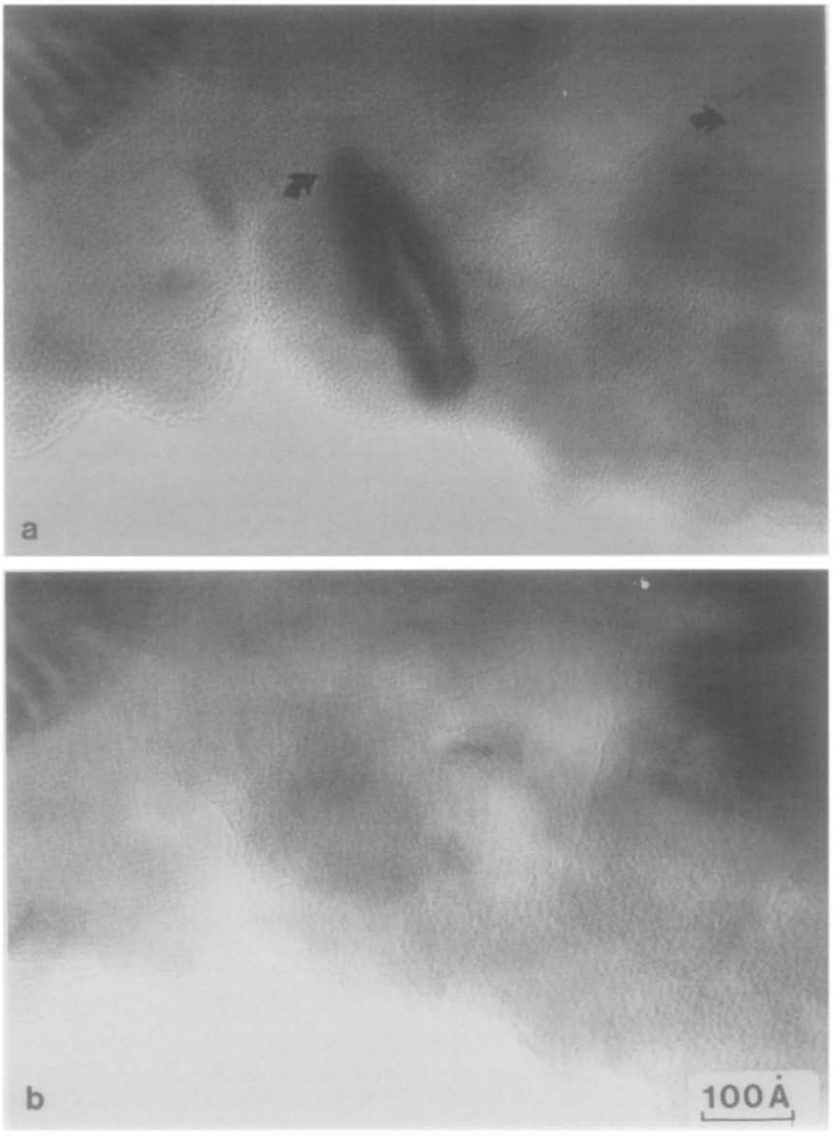

FIG. 14. Image showing an ovoid blob in an amorphous area of the material (a). The defect disappears after a prolonged electron irradiation (b).

Lattice fringes can also be observed in the core of the defect, but they are rather less disturbed. The origin of such contrast variations should probably be correlated to internal stresses caused by the incident particles.

The second type of defect has been pictured in Figs. 13 and 14. It consists of blobs, similar to those due to precipitates; it must be outlined that they always form in the amorphous areas of the samples. When they appear as round dots (Fig. 13), with a 50- to 200-Å diameter, they are not altered by the electron beam heating. However, when they have an ovoid shape they disappear under the electron beam after a prolonged observation. Such an example is given in Fig. 14: in these micrographs, the contrast of the bulk corresponds to that of amorphous material, without any apparent cristallinity, except in the arrowed zones and in the top of the blob. Under the electron irradiation, the ovoid blob has disappeared.

Conclusion

The HREM study of irradiated barium hexaferrite shows clearly that heavy ion bombardment induces numerous defects in the structure in the low-energy range of the ions.

Extended defects, disordered and amorphized zones have been observed in the bulk explaining changes of the magnetic properties as previously reported (*2*). Further investigations of samples irradiated with higher doses (about 10^{14} and 10^{15} ions $\cdot$ cm^{-2} for Kr and Ar, respectively) taking into account their localization with respect to the ion path are in progress in order to define the relative influence of the electronic and atomic energy losses in the radiation damages.

Acknowledgments

The authors are indebted to J. Dural and J. M. Ramillon (CIRIL, Caen) for their efficient technical assistance during the irradiations and to E. Balanzat, J. C. Jousset, and M. Toulemonde (CIRIL, Caen) for helpful discussions. Acknowledgments are also addressed to J. P. Ganne (Thomson-CSF, Orsay) for supplying the single-crystal samples of $BaFe_{12}O_{19}$.

References

1. D. A. Thompson, *Radiat. Effects* **56,** 105 (1981).
2. D. Groult, M. Hervieu, N. Nguyen, B. Raveau, G. Fuchs, and E. Balanzat, *Radiat. Effects*, **90,** 191 (1985).
3. J. C. Jousset, *Ann. Chim.* **9,** 373 (1984).
4. F. Hubert, A. Fleury, R. Bimbot, and D. Gardes, *Anphaj* **5** (Suppl.) 1 (1980).
5. L. C. Northcliffe and R. F. Schilling, *Nuclear Data Tables* **7,** 233 (1970).
6. J. Van Landuyt, S. Amelinckx, J. A. Kohn, and D. W. Eckart, *J. Solid State Chem.* **9,** 103 (1974).
7. F. J. A. Den Broeder, *J. Solid State Chem.* **37,** 362 (1981).
8. Y. Hirotsju and H. Sato, *J. Solid State Chem.* **26,** 1 (1978).
9. S. Amelinckx, R. Gevers, and J. Van Landuyt, "Diffraction and Imaging Techniques in Material Science," Vol. 1, p. 355, Elsevier, New York (1978).
10. G. Van Tendeloo, D. Van Dyck, J. Van Landuyt, and S. Amelinckx, *J. Solid State Chem.* **27,** 55 (1979).
11. L. Ganapathi, J. Gopalakrishnan, and C. N. R. Rao, *Mat. Res. Bull.* **19,** 669 (1984).
12. H. W. Zandvergen, F. C. Mijlhoff, D. J. W. Ijdo, and G. Van Tendeloo, *Mat. Res. Bull.* **19,** 1443 (1983).
13. T. Yoshiie, C. L. Bauer, and M. H. Kryder, *IEEE Trans. Magn.* **MAG-19,** 1823 (1983).
14. B. Strocka, P. Hansen, and H. Heitmann, *Radiat. Effects* **72,** 219 (1983).